Preprint typeset using LaTeX style emulateapj v. 5/2/11

arXiv:1410.3391v2 [astro-ph.EP] 4 Nov 2014

MIGRATION AND GROWTH OF PROTOPLANETARY EMBRYOS I: CONVERGENCE OF EMBRYOS IN PROTOPLANETARY DISKS

Xiaojia Zhang[1*], Beibei Liu[2], Douglas N. C. Lin[1,3], Hui Li,[4]

ABSTRACT

According to the core-accretion scenario, planets form in protostellar disks through the condensation of dust, coagulation of planetesimals, and emergence of protoplanetary embryos. At a few AU in a minimum mass nebula, embryos' growth is quenched by dynamical isolation due to the depletion of planetesimals in their feeding zone. However, embryos with masses (M_p) in the range of a few Earth masses ($M_\oplus$) migrate toward a transition radius between the inner viscously heated and outer irradiated regions of their natal disk. Their limiting isolation mass increases with the planetesimals surface density. When $M_p > 10M_\oplus$, embryos efficiently accrete gas and evolve into cores of gas giants. We use numerical simulation to show that, despite streamline interference, convergent embryos essentially retain the strength of non-interacting embryos' Lindblad and corotation torque by their natal disks. In disks with modest surface density (or equivalently accretion rates), embryos capture each other in their mutual mean motion resonances and form a convoy of super Earths. In more massive disks, they could overcome these resonant barriers to undergo repeated close encounters including cohesive collisions which enable the formation of massive cores.

Subject headings: planetary systems: formation - planetary systems: protoplanetary discs

1. INTRODUCTION

Since the discovery of 51 Pegasi b (Mayor & Queloz 1995), more than 10^3 planets orbiting stars other than the Sun have been detected and confirmed. Exoplanet observations implicate that nearly $15-20\%$ of solar type stars harbor at least one gas giant planet with mass (M_p) comparable or larger than that of Saturn (Marcy et al. 2008; Cumming et al. 2008). Despite the observational bias against the detection of additional long-period and low-mass companions, a large fraction of the known gas giants reside in multiple-planet systems (http://exoplanet.eu/catalog-all.php). Both radial velocity and transit surveys lead to the discovery of a much richer population of super Earths (Mayor et al. 2011; Howard et al. 2012; Batalha et al. 2013; Fressin et al. 2013; Petigura et al. 2013). These findings pose a constraint on the theory of planet formation.

The widely adopted core accretion scenario is based on the assumption that planet formation proceeded through dust condensation and aggregation, planetesimal coagulation, and embryo mergers within their gaseous natal disks (Lissauer 1993; Goldreich et al. 2004; Dullemond & Dominik 2005). This growth is quenched when the embryos acquire an isolation mass ($M_{\rm iso}$) through the consumption of most planetesimals within their feeding zones (Lissauer 1987; Kokubo & Ida 1998). At a few AU in a minimum mass nebula (MMN), $M_{\rm iso} \sim$ is a few Earth mass ($M_\oplus$) but below the critical mass $M_{\rm crit}(\sim 10M_\oplus)$ (Pollack et al. 1996). Although $M_{\rm iso} > M_{\rm crit}$ well beyond the snow line, embryos growth time scale in the outer disk regions is likely to exceed the observed disk depletion time scale ($\tau_{\rm dep} \sim 3-5$ Myr) (Ida & Lin 2004).

The magnitude of $M_{\rm iso} \propto \Sigma_p^{3/2}$ where Σ_p is the surface density of the building block planetesimals. The growth barrier can be bypassed with either an initial Σ_p a few times larger than that of the MMN model or new supplies of grains, planetesimals, or embryos to replenish the feeding zones. Potential transport mechanisms include hydrodynamic drag of grains (Weidenschilling 2003) and vortice-trapping of pebbles (Johansen & Lacerda 2010). In this paper, we focus our discussion on the type I migration of embryos as the dominant mechanism to redistribute embryos' building block materia l(Alibert et al. 2005).

Embryos excite density waves in the disk which carries flux of angular momentum (Goldreich & Tremaine 1982). When these waves are dissipated, they induce both differential Lindblad and corotation torque. Linear calculations indicate that although Earth-mass embryos do not significantly modify the disk structure, their angular momentum exchange with the disk can lead to rapid type I migration (Ward 1997; Tanaka et al. 2002; Kley & Nelson 2012; Baruteau et al. 2013). At 5 AU in a MMN (where Jupiter resides today), differential Lindblad torque alone leads to the inward migration of critical mass cores over a time scale $\tau_{\rm mig} < \tau_{\rm dep}$. Such a rapid migration rate would not only reduce the retention efficiency of cores but also suppress the formation of gas giants at a few AU (Papaloizou & Nelson 2005b).

Several mechanisms to reduce the rate of type I migration have been suggested. They include stochastic migration in turbulent disks (Papaloizou & Nelson 2005a), "planet-trapping" by disk region with positive surface density gradient (Masset et al. 2006; Morbidelli et al. 2008) or by vortices generated from Rossby wave instabilities (Koller et al. 2003; Li et al. 2009), and stalling migration at the inner disk edge (Terquem & Papaloizou

* E-mail: xzhang47@ucsc.edu
[1] Department of Astronomy and Astrophysics, University of California, Santa Cruz, CA 95064, USA
[2] Kavli Institute for Astronomy & Astrophysics and Department of Astronomy, School of Physics, Peking University, Beijing 100871, China
[3] Institute for Advanced Studies, Tsinghua University, Beijing 100084, China
[4] Los Alamos National Laboratory, Los Alamos, NM 87545, USA

2007; Pierens & Nelson 2008).

The most promising mechanism to quench type I migration is contribution by a corotation torque due to an embryo's interaction with nearby gas which follows a horseshoe pattern in its corotating frame. The magnitude and sign of the corotation torque are determined by either the gas surface density (Σ_g) or entropy (S_g) gradient in the horseshoe region (Paardekooper & Mellema 2006; Kley & Crida 2008). In the viscously heated inner and irradiated outer unperturbed regions of the disk, embryos' corotation torque is more intense than their differential Lindblad torque and has respectively positive and negative signs with the potential to induce their outward/inward migration (Kretke & Lin 2012).

However, relatively massive embryos significantly perturb the disk stream lines, reduce their advective transport of angular momentum, and trap them within the horseshoe region (with a width $\Delta a_{\rm hr}$). On a liberation time scale ($\tau_{\rm lib}$), mixing of the gas reduces the Σ_g or S_g gradients and weakens (saturates) the corotation torque (Balmforth & Korycansky 2001). Nevertheless, turbulence in the disk also induces an intrinsic outward transport of angular momentum which enables gas 1) to flow through the horseshoe region of embryos with modest masses, 2) to preserve the Σ_g and S_g distribution, and 3) to retain the corotation torque (Paardekooper et al. 2010; Baruteau & Lin 2010; Paardekooper et al. 2011). Around low-mass embryos, the time scale for the disk gas to diffuse through $\Delta a_{\rm hr}$ is much smaller than $\tau_{\rm lib}$ such that a large fraction of the gas diffuses through their horseshoe regions without being perturbed by their gravity. In the high-mass limit, the vortensity and entropy related part of corotation torque is saturated. In the low-mass limit, the magnitude of corotation torque approaches the linear corotation torque which is below those of differential Lindblad torque. The embryos would undergo inward migration throughout the disk.

Within certain mass range ($\sim$ a few $M_\oplus$), embryos undergo convergent type I migration towards transitional radii ($r_{\rm trans}$) where the net (Lindblad plus corotation) torque changes sign with a negative radial gradient. It has been suggested this process may lead to the accumulation of building block material and enhance the growth of embryos (Nelson 2005; Lyra et al. 2010; Paardekooper et al. 2011; Horn et al. 2012; Hellary & Nelson 2012). Pierens et al. (2013) investigated the effects of initial number of embryos and the stochastic force on the frequency of Gas Giants formation. They suggested that the resonant chain can be broken by increasing the initial number of embryos or by including a moderate stochastic force due to the disk turbulence. They also discussed briefly about the dependency of zero-torque radius on the protoplanetary disk mass, but the effects of different disk mass on convergent migration of embryos were not discussed. In this paper, we emphasize on this potential mechanism and explore conditions under which the critical mass cores ($\sim 10 M_\oplus$) may form and be retained during the main course of disk evolution. After we submitted our paper, a paper by Coleman & Nelson (2014) was posted on Arxiv.org. They investigated the correlation between initial disk mass and the formation and survival of gas giants, and pointed out that in order to form and retain gas giants, it is necessary for planetary cores to accrete gas and open gap at large radii and they must do it in a sufficiently late epoch to prevent migrating into the central star. However, during this advanced stage, much of the initial disk mass is depleted from its initial values so that the critical condition for cores retention by their natal disks is not yet explicitly determined. Although we obtain some similar results on the condition for multiple embryos to overcome resonant barriers (as found by Coleman & Nelson (2014)), our consideration of more general boundary conditions in this and subsequent papers bypass some retention issues associated with their corotation saturation. Following previous work, we use in the paper a 2D FARGO code to carry out hydrodynamic simulation of tidal interaction between multiple embryos and their natal disks. In §2, we briefly recapitulate the numerical method and model parameters.

Following the detailed analysis by Paardekooper et al. (2010, 2011), we verify in §3 that in disks with *composite* Σ_g distribution, isolated embryos undergo the type I migration to $r_{\rm trans}$. These simulations are extended to multiple embryos in §4. Since contribution from corotation torque determines the direction of type I migration, we introduce an idealized model to examine whether it may be affected by overlapping horseshoe regions between two nearby embryos. In this model, we neglect mutual gravitational interaction between embryos and trace diffusion across the corotation zone with passive contaminants.

As they approach each other, embryos perturb each other through secular and resonant interaction. These effects are restored in the models presented in §5. We show that in disks with modest Σ_g, convergent embryos are trapped into their mutual mean motion resonance. But embryos' rate of type I migration increases with Σ_g and in relatively massive disks they bypass the resonant barrier.

After their orbits cross, embryos undergo close encounters. We show in §5 that although some embryos scatter each other to location outside the corotation zone, they resume their convergent type I migration. These embryos are entrenched near $r_{\rm trans}$ by persistent type I migration and undergo repeated close encounters until they collide with each other. In the 2D simulations, physical collisions occur within a few hundred orbital periods. However, if the embryos have an nearly isotropic velocity dispersion rather than mono layer distribution, their collision time scale is 2-3 order of magnitude longer, ie a significant fraction of the (Myr) disk evolution time scale. It is impractical to carry out high-resolution hydrodynamic simulation of embryos' close interaction during various stages of disk evolution. In a subsequent paper, we will utilize a prescription for embryo-disk interaction to construct a Hermit-Embryo scheme. This prescription was constructed by Paardekooper et al. (2010, 2011) based on the results of a comprehensive series of hydrodynamic simulations of the embryos-disk interaction. This approximation is justified under the assumption that embryos do not strongly modify the disk's intrinsic structure. Based on the results here, we assume this prescription remains valid for individual embryos in multiple systems. Finally, in §6, we summarize our results and discuss their implications.

2. HYDRODYNAMIC SIMULATION OF EMBRYOS-DISK INTERACTION

Here, we briefly recapitulate the numerical method and model parameters.

Following previous investigations, we utilize a publically available FARGO (Fast Advection in Rotating Gaseous Objects; Masset (2000)) scheme to simulate the interaction between multiple embryos with their natal disks. FARGO is a 2D hydrodynamical polar grid code centred on the star, based on the van Leer upwind algorithm on a staggered mesh. It solves the Navier-Stokes and continuity equations for a Keplerian disk subject to the gravity of the central object and that of embedded protoplanets as well as the energy equation in its more recent version (Baruteau & Masset 2008). The energy equation implemented in FARGO is:

$$\frac{\partial e}{\partial t} + \vec{\nabla} \cdot (e\vec{v}) = -P\vec{\nabla} \cdot \vec{v} + Q_+ - Q_- \qquad (1)$$

where e is the thermal energy density (thermal energy per unit area), $\vec{v}$ is the flow velocity, P is the vertically integrated pressure, and $Q_+(Q_-)$ denote heating (cooling) source terms, assumed to be positive quantities. The cooling source is defined by a cooling time, the disk will go back to the initial energy within the given cooling time. Here we choose the cooling time to be about 5 orbital periods of the planet at $r = 1$.

There're several boundary conditions available in the FARGO code. Here we choose the EVANESCENT boundary condition which is described in de Val-Borro et al. (2006), used for the EU test comparison problem. It aims at implementing wave killing zones at each edge of the grid. It allows the disk values (surface density, velocities, thermal energy density) to damp toward the instantaneous axisymmetric disk conditions. The damping regions are located in the radial ranges $[r_{min}, 1.25r_{min}]$ and $[0.84r_{max}, r_{max}]$, where $r_{min}(r_{max})$ denotes the inner (outer) edge radius of the grid.

The basic equations are solved in a cylindrical coordinates from $r = 0.3$ to $r = 1.7$ and full 2π in azimuth. The typical resolution is $\delta r/r_p \sim 0.004$ and $\delta\phi = 0.01$, which gives about 5 grids in radial direction within the Hill's radius of a $10M_\oplus$ planet.

For illustration, we adopt a simple α disk model with an effective viscosity. We assume power-law distributions

$$\frac{\partial ln\Sigma_g}{\partial lnr} = p, \qquad \frac{\partial lnT}{\partial lnr} = q, \qquad \frac{\partial ln\alpha}{\partial lnr} = \zeta. \qquad (2)$$

In a steady state, the accretion rate $\dot{M} = 3\pi\Sigma_g\alpha{C_s}^2\Omega$ is independent of r so that $p + q + \zeta = -1.5$.

We adopt a disk model based on the assumption that the inner region of the disk is heated by viscous dissipation whereas the outer region is heated by stellar luminosity (Garaud & Lin 2007). we set the transit region at r_t, the disk inside r_t has $p = 0.0$ and $q = -1.5$ and outside has $p = -0.5$ and $q = -1.0$. In the simulations, these model parameters follow a continuous transition at r_t. This composite power-law Σ_g and T distribution model is an extension of the single power-law simulations pioneered by Paardekooper et al. (2010, 2011).

We simulate the planetary migration in disks of both high and low accretion rate to investigate the dependency of orbital structure on the convergent migration rate. According to the disk model structured by Garaud & Lin (2007), $h/r \propto \dot{M}^{0.25}$ and $r_t \propto \dot{M}^{0.72}$. For normalization, we specify $h/r = 0.079$ at r_t for a disk with accretion rate as high as $10^{-7}M_\odot yr^{-1}$, and $h/r = 0.05$ at r_t for $1.2 \times 10^{-8}M_\odot yr^{-1}$ (model 5). To reduce the simulation time for planetary migration in low $\dot{M}$ disks, we set $r_t = 7.1$ AU for all disk models. The viscosity α is 0.001 as constant, and the smoothing length $b/h = 0.4$.

TABLE 1

model	N_p	$M_p(M_\oplus)$	$\dot{M}(M_\odot yr^{-1})$	feel others	feel disk
1a-1c	1	10	1e-7	NO	YES
1d	1	20	1e-7	NO	YES
1e	1	30	1e-7	NO	YES
1f	1	40	1e-7	NO	YES
1g	3	10	1e-7	NO	YES
5	4	10	1.2e-8	YES	YES
6a	4	10	1e-7	YES	YES
6b	4	10	2e-7	YES	YES

feel other: gravitational interaction with other planets.
feel disk: interaction between planet and disk.

We first simulate the migration of a single isolated planet in a disk of composite Σ_g or S_g distributions to confirm that the planets would undergo convergent migration in this kind of disk model (model 1a-1f). Then we compare the results with the migration of a single planet in a disk disturbed by other planets (model 1g). At last, we simulate the migration of multiple planet systems in disks with different accretion rates (model 5 & 6). In all models, the planet has initial circular orbit. The model parameters are listed in Table 1.

3. MIGRATION OF SINGLE ISOLATED PLANETS

The planet with $M_p = 10M_\oplus$ migrate outward when released inside the transit location (model 1a) and migrate inward when starting outside (model 1c) (Fig. 1). The sign and magnitude of the initial torque agree well with that obtained for a planet in a disk with a single power-law Σ distribution. In both cases, the migration is slowed down and stalled when the planet approaches r_t. Although the strength of one-side torque is preserved, the net Lindblad torque is suppressed by the cancellation from the two regions of the disk. The reduction of the differential Lindblad torque enables it to balance the corotation torque. These models indicate that in disks with a bimodel (p, q) distribution, the net torque can indeed be summarized as a linear combination of that from two separate regions of the disk.

In model 1d-1f, we place a single isolated planet at initial location $r = 0.8$ with $M_p = 20M_\oplus$, $30M_\oplus$ and $40M_\oplus$ respectively. The planet migrated outward with stalling at r_t in model 1d and migrated inward in model 1e and 1f (Fig. 1). For this M_p, perturbation on Σ_g remains relatively small. These results are in general agreement with those obtained by Paardekooper et al. (2010, 2011) and they indicate that the corotation torque of massive planets is saturated (weakened) by the suppression of diffusion of disk gas across the horseshoe stream lines.

4. MIGRATION OF MULTIPLE PLANETS

When two or more planets converge near r_t, the location of their Lindblad resonances and horseshoe region may overlap with each other. They also directly interact with each other. We assess the relative contribution

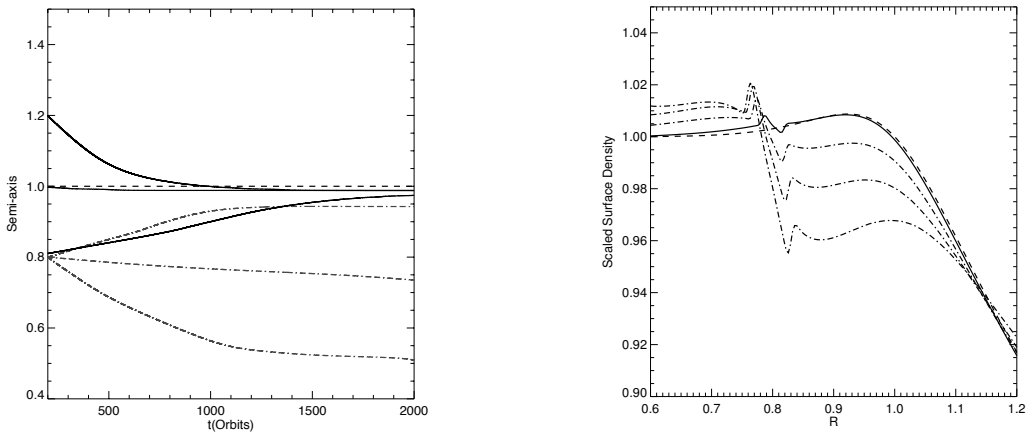

FIG. 1.— **Left panel**: The three solid lines indicate the semi-axis evolution of a $10M_\oplus$ planet released from $r = 0.8$, $r = 1.0$ and $r = 1.2$ respectively(model 1a-1c). The three dot-dashed lines indicate the semi-axis evolution of a planet from $r = 0.8$ with mass of 20, 30 and $40M_\oplus$ respectively(model 1d-1f). The dashed line indicates the location of r_t. **Right panel**: Surface density profile scaled with unperturbed $\Sigma(r_t)$. The dashed line indicates the profile of unperturbed disk. The solid and three dot-dashed curves, with value at r_t from higher to lower, indicate that disturbed by a planet with mass of 10, 20, 30 and $40M_\oplus$ respectively(model 1a, 1d-1f) after 200 orbits.

from different effects with idealized simulations of the concurrent evolution of multiple planets.

We first examine the extent of resonant interference by releasing three planets at the same location as the previous single-planet models. In an artificial, idealized model, we neglect the mutual interaction between the planets (model 1g). Initially, the disk response is a linear combination perturbation of three widely separated planets. These planets independently evolve along paths similar to those of the analogous individual planets (Fig. 2). As they approach r_t, their combined perturbation amplitude on the disk is locally enhanced, albeit changes in Σ_g remains small and linear (Fig. 2).

In order to further investigate the interference of planets on each other's migration, we introduce a tracer (as passive contaminant) to highlight the diffusion of fluid elements around the planets when they are very close to each other. For comparison, the fluid elements' tracer is examined under four situations: (model 0) an unperturbed disk (without any embedded planet), (model 2a) a disk which bears a single planet with a fixed position at $R = 1.0$, (model 3a) disk with two planets fixed at $R = 1.0$ and $R = 1.1$ and (model 4a) disk with two planet at $R = 1.0$ and $R = 0.9$. Figure 3 shows the diffusion pattern of tracer elements under these 4 cases with $M_p = 10M_\oplus$. Models 1a-4a are presented from top to the bottom rows. The tracer distribution at time 0, 400, and 800 orbital period are plotted in left to right columns.

Comparisons between models 0 and 2a highlight the horse shoe stream lines near the corotation region around an embedded planet. Width of the corotation zone around the $10M_\oplus$ planet is ~ 0.05. In models 3a and 4a, the corotation zones of the two planets are adjacent to each other without any significant overlap. Nevertheless, their co-existence leads to weak diffusion to either outer (model 3a) or inner (model 4a) regions.

Figure 4 shows the tracer distribution for models (2b-4b) with $M_p = 20M_\oplus$ (in rows 1-3). Columns 1 and 2 (from the left) represent the distribution after 400 and 800 orbits. Similar models (2c-4c) with $M_p = 2M_\oplus$ at the corresponding epochs are plotted in columns 3 and 4 (from the left).

The corotation region around a $2M_\oplus$ planet (model 2c) is ~ 0.02. The corotation regions around the coexisting planets in models 3c and 4c are well separated. There is no evidence of horse shoe stream line interference to enhance the diffusion of tracer elements.

In contrast, model 2b shows that around a $20M_\oplus$ planet, the width of the corotation region is ~ 0.07 such that two planets with 0.1 separation have overlapping corotation regions. The horse shoe stream lines around two planets are clearly intertwine in models 3b and 4b. Gravitational perturbation from the exterior planet enhances outward diffusion whereas that from the interior planet promotes more rapid inward migration.

In previous analysis, Paardekooper et al. (2010, 2011) showed that the preservation of the Σ_g profile near the embedded planets and the maintenance of their corotation torque require gas diffusion through the corotation region. For relatively large planets, the diffusion is quenched by the horse shoe streamlines and saturates the corotation torque. The elevated diffusion of tracer elements in disks with closely packed multiple planets (models 2c and 2d) limits the modification of the unperturbed Σ_g distribution and unsaturates the corotation torque in comparison with that between the disk and isolated planets (model 2b).

Our simulated models suggest that 1) the migration direction, pace and the net torque of individual planets are not affected by other planets in well separated multiple systems and 2) closely-packed multiple planets also retain their unsaturated corotation torque. Thus, resonant interference enhances rather than suppresses convergent migration. Based on these results, we approximate, in subsequent papers of this series, the torque exerted by individual planets in multiple systems with the prescription obtained from simulations with single planets (Paardekooper et al. 2010, 2011).

5. GRAVITATIONAL INTERACTION AND MERGER THROUGH PHYSICAL COLLISIONS

We now incorporate the gravitational interaction between planets. We place four equal-mass ($10M_\oplus$) planets into the disk (with the same p, q distribution as previous

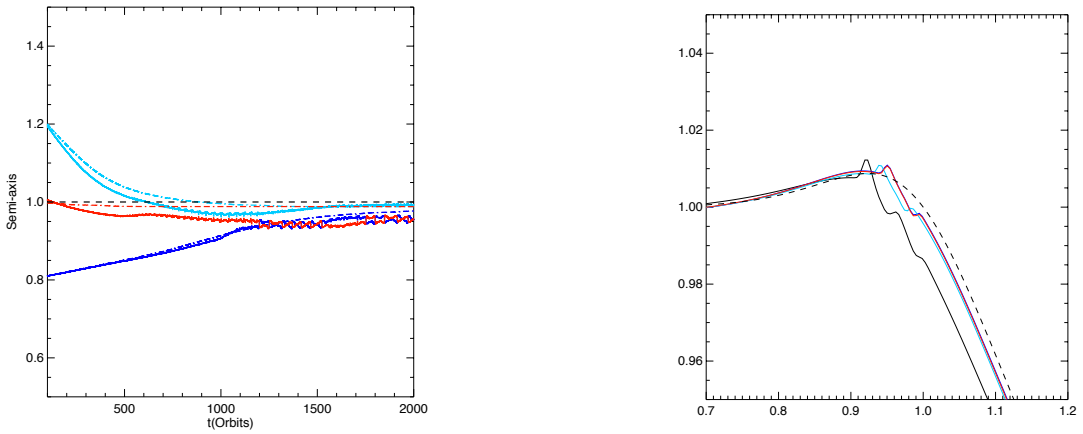

FIG. 2.— **Left panel:** The semi-axis evolution of three planets with equal mass of $10M_{\oplus}$ (model 1g). The planets are released from $r = 0.8$ (dark blue solid), $r = 1.0$ (red solid) and $r = 1.2$ (light blue solid). During their migration, planets' direct gravitational perturbation on each other is neglected. However, the disk is perturbed by all three planets. The dot-dashed color lines represent the migration with single planets from previous comparison models 1a-1c. The dashed black line indicates the location of r_t. **Right panel:** The dashed solid and black lines represent the surface density profile at $t = 0$ and $t = 2000$ orbits in the case of multi-planets' migration respectively. The color lines represent the surface density profile at $t = 2000$ orbits of the previous three separate cases of isolated planet's migration.

models) at $r = 0.7, 0.9, 1.1, 1.3$ respectively.

In model 5, we specify a low-mass disk with $\dot{M} = 1.2 \times 10^{-8} M_{\odot} yr^{-1}$. In this case, the embryos rapidly capture each other on their 6:5 or 5:4 mean motion resonances (Fig. 5). This resonant configuration is maintained with a fluctuating eccentricity $e \sim R_R/a \sim 0.02$ while the convoy's inward migration slows down and comes to a halt. In this compact configuration, the periastron of some embryos crosses the apoastron of other embryos which are slightly closer to their host stars. After 1300 orbits, two middle embryos' orbit overlapped and they exchange their orbit to re-establish the resonant configuration. In general the embryos preserve their integrity and may undergo further migration together as the disk is depleted. We suggest that these convoys are the progenitors of multiple super Earths.

We also introduce models 6a and 6b with similar embryos' mass and initial location as model 5. But the gas accretion in the disk is specified to be 10^{-7} and $2 \times 10^{-7} M_{\odot} yr^{-1}$ respectively.

Similar to the results of model 5 and our previous simulation (Zhang et al. 2014), embryos in model 6a first capture each other into lower-order mean motion resonances. During their subsequent collective migration, their separation is reduced to about half of their initial spacing. Embryos' e fluctuates mostly with an average amplitude < 0.02 as it is excited by the embryos' resonant interaction with each other and damped by the tidal torque between them and the gas. Since their separation is $\sim 0.1 r_p$, their orbits do not generally cross each other. But, on some occasions (eg at ~ 300 orbits), pairs of closest embryos may become dynamically unstable to undergo orbit crossing. Close encounters lead to the exchange of semi major axes and eccentricity excitation ($\sim R_R/a$ up to ~ 0.05) (Fig. 6). After this brief episode of close encounters and intense interaction, embryos' eccentricity is quickly damped by the tidally induced gas drag from the disk gas.

A convoy of embryos settles near but not precisely around r_t. This slight asymmetry is due to the embryos' torque balance between the inner and outer regions of the disk. After ~ 700 orbits, the two inner most embryos again cross each other's orbit and exchange their semi major axes. Models 5&6a indicate the possibility of repeated orbit crossing. Since embryos would undergo orbit crossing when their separation is smaller than the width of feeding zone (Zhou et al. 2007), under some circumstances, the embedded embryos may converge into regions where they undergo repeated close encounters. Some encounters may be sufficiently close that the participating planets physically collide and merge with each other. In this series of papers, we will explore the possibility that these merger may attain critical mass for the onset of efficient gas accretion. In order to simulate this possibility with FARGO, we remove the gravitational softening parameter in the calculation of the force between the participating embryos and assume they would merge with each other, with the conservation of mass and momentum, if their impact parameter is smaller than a critical merger size $R_c \simeq 4R_p$.

In a previous analysis (Zhang et al. 2014), we showed that the embryos' convergent type I migration is halted with an interplanetary spacing Δa which is a decreasing function of $\dot{M}$. In a steady disk with a constant α, Σ_g generally increases with the accretion rate $\dot{M}$. The strength of both differential Lindblad and corotation torque as well as the embryos' type I migration speed increase with Σ_g. We introduce model 6b to show that in disks with relatively large Σ_g (or equivalently $\dot{M} = 2 \times 10^{-7} M_{\odot}$ yr^{-1}), the embryos undergo the similar paths as that in the previous models.

We find that, the faster convergent migration rate leads to the merge of the middle two embryos shortly after released. Later they converged into a resonant state (Fig. 6). If we use the embryos' actual physical size R_p with a comparable density as the Earth, the estimated collision time scale would be $\tau_c \sim (a\delta a/NR_p^2\Theta)P$, which is several orders of magnitude longer than their orbital period P even after they converge into a region with a radial width δa comparable to their Roche radius or the extent of their corotation region. However, under the 2-D disk simulations, the collision frequency is much higher,

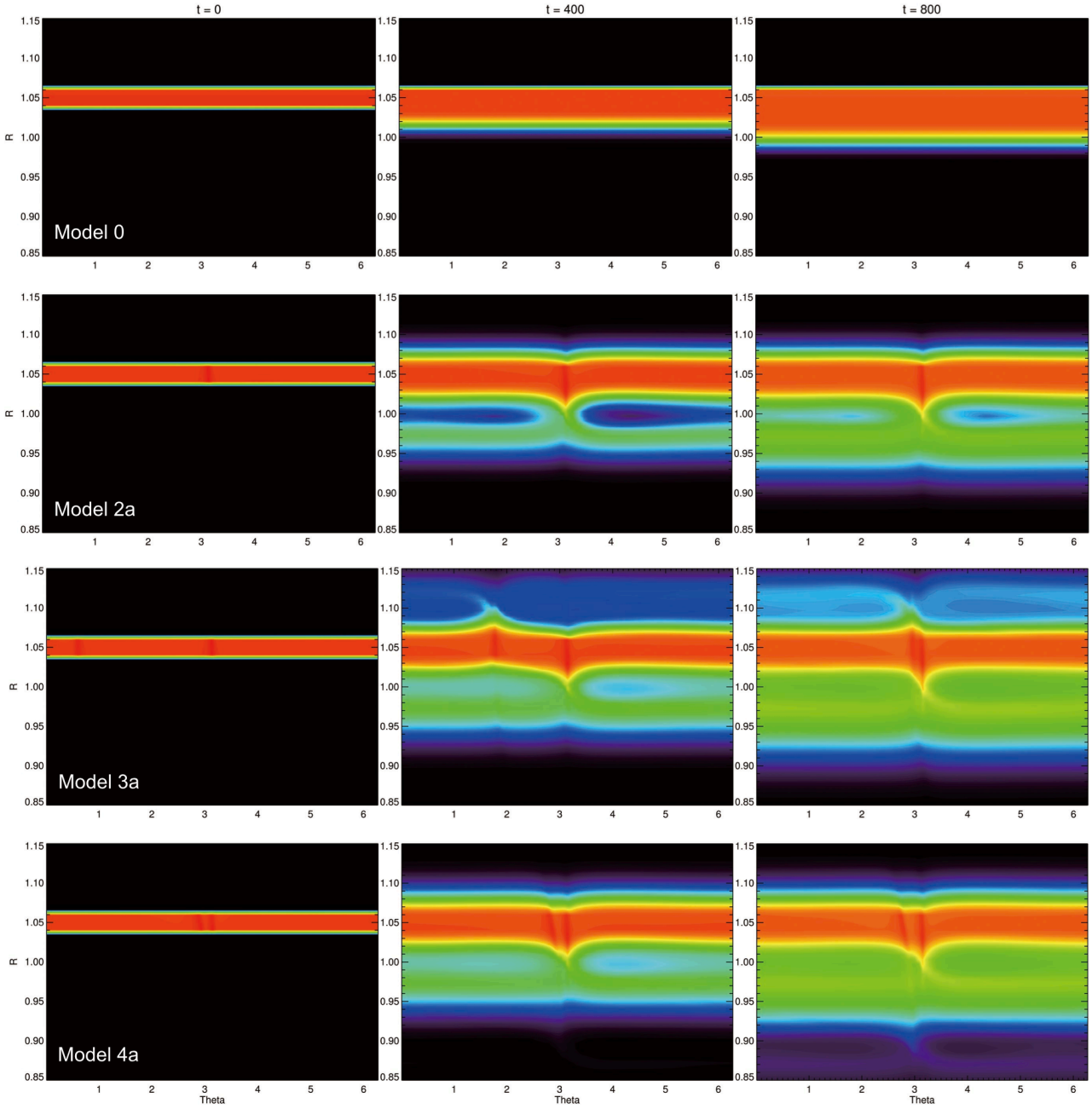

FIG. 3.— Diffusion of tracer elements in an unperturbed disk model 0 (**row 1**), a disk with one planet fixed at r_t in model 2a (**row 2**), a disk with two planets fixed outside r_t in model 3a (**row 3**), and two planets fixed inside r_t in model 4a (**row 4**). All the planet has equal mass as $10M_\oplus$. The left column represents the initial tracer distribution. The middle and right columns represent the tracer distribution at t=400 and 800 orbits.

the orbital crossing time scale could be reduced to several hundred orbital period. Realistic collisions require protracted simulations which is beyond the current computational constraint.

The total mass of the embryos (40 $M_\oplus$) in models 5, 6a and 6b exceeds M_p ($= 20M_\oplus$) in models 1d-1f (see §3). Yet, this convoy of resonant embryos are retained near r_t whereas the more massive isolated embryo migrated toward the inner boundary of the disk. These results indicate that, as separate entities, lower-mass embryos preserve their corotation torque (in model 6a). But if they merge into sufficiently massive isolated embryos, their corotation torque would be saturated and they may no longer be trapped near r_t (model 6b). After the merger event, the massive embryo continues to migrate inward. Its perturbation on the disk structure is enhanced. In isolation, the merger's mass is sufficiently large for it to confine the horse shoe stream lines and saturate the corotation torque. As we have shown in §4, the interference by other nearby embryos induces mixing of stream lines and restores diffusion across their corotation regions.

6. DISCUSSION AND SUMMARY

In the sequential accretion scenario, the formation of critical mass cores (with $M_p > M_c \sim 10M_\oplus$) prior to the severe depletion of gas in protostellar disks is a prerequi-

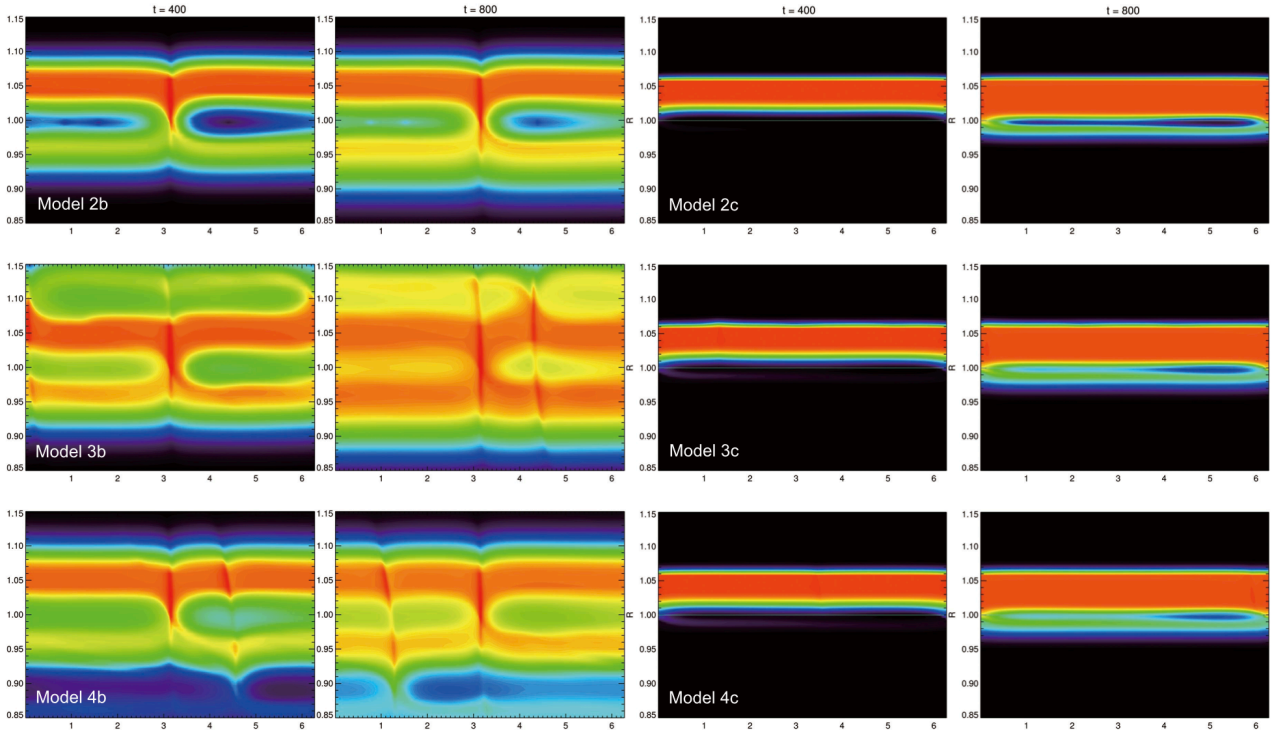

FIG. 4.— Diffusion of tracer elements for models 2b-4b (**rows 1-3**) with 20 $M_\oplus$ planets after 400 and 800 orbits in columns 1 and 2 from the left. Similar disk models 2c-4c with 2 $M_\oplus$ planets after 400 and 800 orbits are shown in columns 3 and 4.

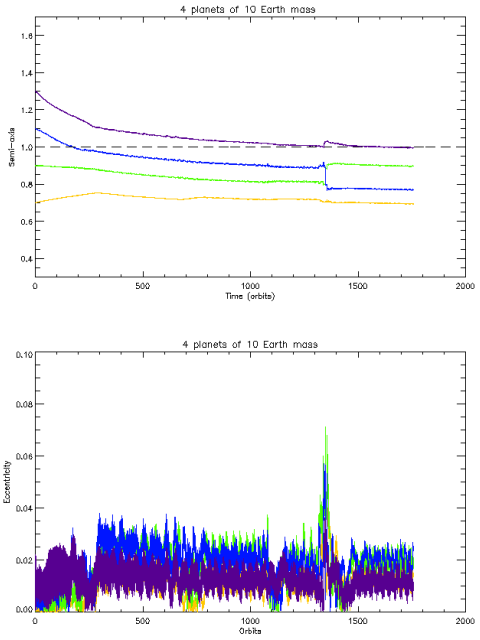

FIG. 5.— The semi-axis (**top**) and eccentricity (**bottom**) evolution of four $10M_\oplus$ planets' orbits released from $r = 0.7, 0.9, 1.1, 1.3$ respectively in a disk of $\dot{M} = 1.2 \times 10^{-8} M_\odot/yr$ (model 5) .

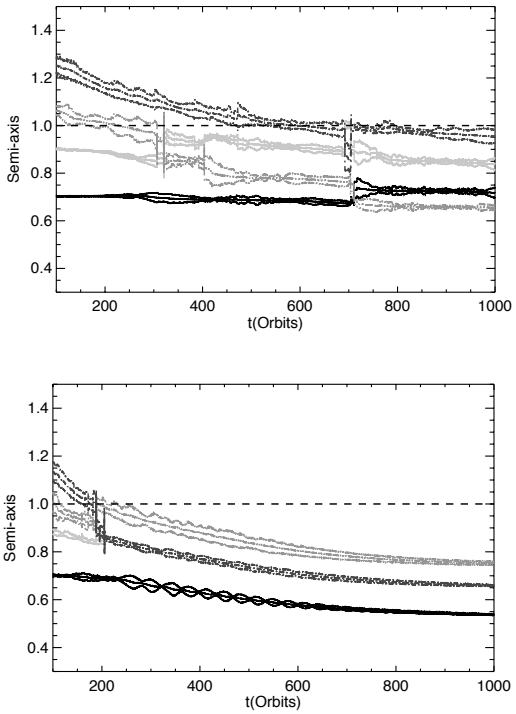

FIG. 6.— The semi-axis and eccentricity evolution of four $10M_\oplus$ planets' orbits released from $r = 0.7, 0.9, 1.1, 1.3$ respectively in disks with different accretion rate. Each group of curves show the paths of a, $a\times(1+e)$ and $a\times(1-e)$ for the same planet. (**Top**: $\dot{M} = 10^{-7} M_\odot/yr$(model 6a), **Bottom**: $\dot{M} = 2 \times 10^{-7} M_\odot/yr$(model 6b)).

site for the formation of gas giant planets. In this paper, we present simulations to examine the condition for the formation of critical mass cores.

We confirm previous hypothesis that the core formation probability is greatly enhanced by the type I migration of protoplanetary embryos. The magnitude and direction of embryos' migration is determined by their net differential Lindblad and corotation torque. In the outer

irradiated regions of protostellar disks, these torques lead to inward migration. But in the inner viscously heated regions of the disk, unsaturated (full strength) corotation torque is stronger than the differential Lindblad torque and it induces an outward migration. However, the corotation torque is suppressed by saturation for both massive ($> 10M_\oplus$) and low-mass ($< 3M_\oplus$) embryos. Nevertheless, super-Earth embryos undergo convergent migration towards the transition radius ($r_t \sim$ a few AUs) which separates these two disk regions.

Here we present numerical simulations to show that the torque prescription previously constructed by Paardekooper et al. (2010, 2011) for idealized single power-law Σ_g and S_g distribution can be generalized to more complex disk models. This applicability is a reflection that the embryo-disk torque is mostly applied to the proximity of the planets orbit over length scales much shorter than that modifies the disk structure.

We show that when multiple embryos congregate near r_t, they interact with each other through secular and resonant perturbations. In disks with modest Σ_g (or $\dot{M}$), the convergent speed is relatively slow. They would capture each other on their mutual mean motion resonances if the resonant liberation time scale is shorter than that for the approaching embryos to cross the resonant width. These planets form a convoy of resonant embryos. The separation between the planets decreases with $\dot{M}$.

In disks with sufficiently large $\dot{M}$, the embryos' separation becomes comparable or smaller than the total width of their mean motion resonance. Interference between horseshoe stream lines around each planet enhances diffusion of gas through the corotation region and suppresses the saturation of corotation resonances. In this limit, embryos converge with overlapping orbits.

Orbit crossing embryos undergo repeated close encounters. Although some embryos are scattered outside the corotation zones, converging type I migration continually repatriate them back to the proximity of r_t. The trapped embryos continue to scatter each other until they undergo physical collision.

The conditions for the collisional products to evolve into a super critical mass core are: 1) there is adequate time for collision to occur, 2) the physical collisions need to be mostly cohesive, and 3) the merger products must be retained. The value of r_t is also an increasing function of $\dot{M}$. In disks with sufficiently large $\dot{M}$ for embryos to bypass the resonant barrier, r_t is at least a few AU where the local Keplerian velocity is smaller than the surface escape speed of super-critical mass cores. Since the embryos' velocity dispersion is much smaller than their Keplerian velocity, their collisions are not sufficiently energetic to cause any significant fragmentation.

The collision time scale for the embryos is expected to be much longer than the orbital period but shorter than the gas depletion time scale. We used an idealized model to simulate the consequence of a merger event on the residual embryos. Hydrodynamic simulations with a realistic collision time scale is beyond the current computational feasibility, especially for a systematic model parameter study. Based on the results presented here, we will present a newly constructed HERMIT-Embryo code to simulate the evolution of multiple embryos in subsequent papers of this series. We will also replace the idealized composite power-law Σ_g distribution with comprehensive evolving disk models.

7. ACKNOWLEDGEMENT

We thank Dr. Clement Baruteau for discussions and technical assistance. We also thank Prof. S. Ida for very useful conversations and an anonymous referee for helpful suggestions in the presentation of this paper. This work is supported by a grant from UC/Lab fee program. We acknowledge support from the LDRD program and IGPPS of Los Alamos National Laboratory.

REFERENCES

Alibert, Y., Mordasini, C., Benz, W., & Winisdoerffer, C. 2005, A&A, 434, 343
Balmforth, N. J., & Korycansky, D. G. 2001, MNRAS, 326, 833
Baruteau, C., & Lin, D. N. C. 2010, ApJ, 709, 759
Baruteau, C., & Masset, F. 2008, in IAU Symposium, Vol. 249, IAU Symposium, ed. Y.-S. Sun, S. Ferraz-Mello, & J.-L. Zhou, 397–400
Baruteau, C., et al. 2013, ArXiv e-prints
Batalha, N. M., et al. 2013, ApJS, 204, 24
Coleman, G. A. L., & Nelson, R. P. 2014, ArXiv e-prints
Cumming, A., Butler, R. P., Marcy, G. W., Vogt, S. S., Wright, J. T., & Fischer, D. A. 2008, PASP, 120, 531
de Val-Borro, M., et al. 2006, MNRAS, 370, 529
Dullemond, C. P., & Dominik, C. 2005, A&A, 434, 971
Fressin, F., et al. 2013, ApJ, 766, 81
Garaud, P., & Lin, D. N. C. 2007, ApJ, 654, 606
Goldreich, P., Lithwick, Y., & Sari, R. 2004, ARA&A, 42, 549
Goldreich, P., & Tremaine, S. 1982, ARA&A, 20, 249
Hellary, P., & Nelson, R. P. 2012, MNRAS, 419, 2737
Horn, B., Lyra, W., Mac Low, M.-M., & Sándor, Z. 2012, ApJ, 750, 34
Howard, A. W., et al. 2012, ApJS, 201, 15
Ida, S., & Lin, D. N. C. 2004, ApJ, 604, 388
Johansen, A., & Lacerda, P. 2010, MNRAS, 404, 475
Kley, W., & Crida, A. 2008, A&A, 487, L9
Kley, W., & Nelson, R. P. 2012, ARA&A, 50, 211
Kokubo, E., & Ida, S. 1998, Icarus, 131, 171
Koller, J., Li, H., & Lin, D. N. C. 2003, ApJlL, 596, L91
Kretke, K. A., & Lin, D. N. C. 2012, ApJ, 755, 74
Li, H., Lubow, S. H., Li, S., & Lin, D. N. C. 2009, ApJ, 690, L52
Lissauer, J. J. 1987, Icarus, 69, 249
—. 1993, ARA&A, 31, 129
Lyra, W., Paardekooper, S.-J., & Mac Low, M.-M. 2010, ApJL, 715, L68
Marcy, G. W., et al. 2008, Physica Scripta Volume T, 130, 014001
Masset, F. 2000, A&AS, 141, 165
Masset, F. S., Morbidelli, A., Crida, A., & Ferreira, J. 2006, ApJ, 642, 478
Mayor, M., & Queloz, D. 1995, Nature, 378, 355
Mayor, M., et al. 2011, in AAS/Division for Extreme Solar Systems Abstracts, Vol. 2, AAS/Division for Extreme Solar Systems Abstracts, 102
Morbidelli, A., Crida, A., Masset, F., & Nelson, R. P. 2008, A&A, 478, 929
Nelson, R. P. 2005, A&A, 443, 1067
Paardekooper, S.-J., Baruteau, C., Crida, A., & Kley, W. 2010, MNRAS, 401, 1950
Paardekooper, S.-J., Baruteau, C., & Kley, W. 2011, MNRAS, 410, 293
Paardekooper, S.-J., & Mellema, G. 2006, A&A, 459, L17
Papaloizou, J. C. B., & Nelson, R. P. 2005a, in Fluid Dynamics and Dynamos in Astrophysics and Geophysics, ed. A. M. Soward, C. A. Jones, D. W. Hughes, & N. O. Weiss, 29
Papaloizou, J. C. B., & Nelson, R. P. 2005b, A&A, 433, 247
Petigura, E. A., Marcy, G. W., & Howard, A. W. 2013, ApJ, 770, 69

Pierens, A., Cossou, C., & Raymond, S. N. 2013, A&A, 558, A105
Pierens, A., & Nelson, R. P. 2008, A&A, 478, 939
Pollack, J. B., Hubickyj, O., Bodenheimer, P., Lissauer, J. J., Podolak, M., & Greenzweig, Y. 1996, Icarus, 124, 62
Tanaka, H., Takeuchi, T., & Ward, W. R. 2002, ApJ, 565, 1257
Terquem, C., & Papaloizou, J. C. B. 2007, ApJ, 654, 1110
Ward, W. R. 1997, Icarus, 126, 261
Weidenschilling, S. J. 2003, Icarus, 165, 438
Zhang, X., Li, H., Li, S., & Lin, D. N. C. 2014, ApJ, 789, L23
Zhou, J.-L., Lin, D. N. C., & Sun, Y.-S. 2007, ApJ, 666, 423